Journal of the Korean Physical Society, Vol. 62, No. 1, January 2013, pp. 40∼47

Optical Structure for a Three-dimensional Liquid-crystal Cell Using a Wide-band and Wide-view Half-wave Retarder

Byung-June Mun and Gi-Dong Lee*
Department of Electronics Engineering, Dong-A University, Busan 604-714, Korea

(Received 13 September 2012, in final form 24 October 2012)

In order to improve the image crosstalk for a film patterned retarder (FPR) of a linear polarizer type in a stereoscopic three dimensional (3D) display, we propose an optical structure with wideband and wide viewing angle characteristics and using only two half-wave retarders. This proposed half-wave retarder of the FPR 3D cell consists of a $\lambda/2$ biaxial film and a patterned $\lambda/2$ A-film. We calculated the phase retardation and confirmed the polarization states of the light passing through each film on the Poincaré over all visible wavelengths by using the Stokes vector and the Muller matrix method. Then, we optimized the optical parameters of the two retardation films in the oblique direction by using the parameter space method as a function of the optical axis and the N_Z parameter of the biaxial $\lambda/2$ film. Consequently, we verified that the left 3D crosstalk of the proposed FPR 3D cell could be improved by about 91.87% in the horizontal viewing direction and 97.22% in the vertical viewing direction. The right 3D crosstalk could almost maintain the crosstalk value of the conventional structure.

PACS numbers: 42.70.Df, 42.79.Kr, 61.30.Cz
Keywords: Stereoscopic 3D display, Film patterned retarder, 3D crosstalk, Wideband, Wide viewing angle
DOI: 10.3938/jkps.62.40

I. INTRODUCTION

Flat panel displays (FPD) have been developed to achieve excellent performances such as low power consumption, high contrast ratio, high definition, and light weight. As a result, the improved FPD technologies have led to a widely-expanding demand for display applications such as TVs, monitors, mobile phones, tablet PCs and so on, but most high vision displays are still limited to the realization of two dimensional (2D) images. Therefore, three-dimensional (3D) displays that can satisfy the requirements of consumers for more realistic images with depth information and vivid pictures have attracted great interest as the next-generation displays [1,2]. In particular, stereoscopic displays with 3D glasses have been proposed as a better selection for home applications and 3D cinemas due to their good display performances and unlimited viewing range. The operating principle of a glass-type 3D display is that a liquid crystal display (LCD) panel sends two difference images to the left and the right eyes of a viewer wearing special 3D glasses in order to produce binocular disparity. There are two major types of the stereoscopic 3D displays. One is a shutter-glass type 3D display, and the other is a film-patterned retarder (FPR)-type 3D display. In the former 3D display, the shutter glasses produce two images corresponding to the left and the right eyes through switching the polarization states synchronized with the 3D displayed images [3–5]. Here, the LCD panel is almost similar to the conventional LCD for 2D images except for the time-division operation to generate the binocular images. In the FPR-type 3D displays, two images with different polarization states corresponding to the left and the right eyes are generated by using the patterned retarder, which is generally attached on the outside of the LCD panel to change the polarization state [6–8]. Currently, this type is greatly preferred by the world 3D market because it is low cost, uses lightweight glasses, has a simple fabrication process, is flicker free, and has wide-viewing angles. However, the FPR 3D display has serious drawbacks such as image quality deterioration and crosstalk at off-normal axis, which is due to an overlap of the left and the right images because the retardation films used in FPR 3D display not only have optical properties that change with the oblique viewing angle, such as a change in the optical axis and a phase retardation, but also can experience a color shift due to wavelength dispersion [9–12].

In general, the 3D LC cell can apply a quarter-wave retarder [13] or a half-wave retarder to separate the left and the right image. In this work, we propose an optical structure using a wide-band and wide-view half-wave retarder for the FPR-type 3D display. The wideband half-wave retarder is composed of a $\lambda/2$ biaxial film and a patterned $\lambda/2$ A-film. Based on the Stokes parameter

*E-mail: gdlee@dau.ac.kr; Fax: +82-51-200-7712

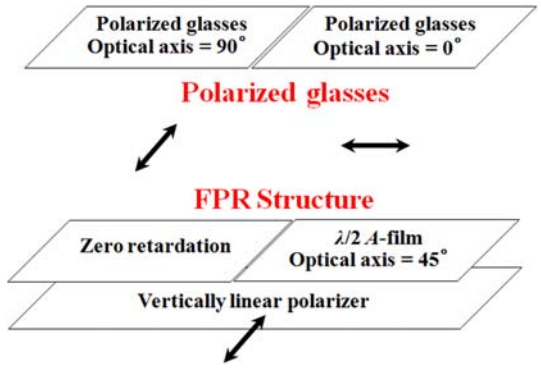

Fig. 1. (Color online) Conventional structure of the FPR 3D display with polarized glasses.

and the Muller matrix method, we calculate the phase retardation of each film over the entire visible wavelength spectrum and analyze the polarization states of the light passing through the optical structure on the Poincaré sphere. By using the parameter space method, we optimize the optical parameters as functions of the optical axis and the N_Z parameter of the biaxial film in the horizontal and the vertical viewing directions (polar angle $\theta = 70°$, which induces maximum light leakage generally [10]) for applications to TV and notebook designs. In order to confirm the enhanced optical characteristics for the proposed FPR structure, finally, we calculate the light leakage and compare the results to the 3D crosstalk for a conventional structure using the TECHWIZ LCD made by SANAYI system.

II. DRAWBACKS FOR THE CONVENTIONAL STRUCTURE OF A FPR 3D DISPLAY WITH A HALF-WAVE RETARDER

Figure 1 shows a conventional optical structure for a FPR stereoscopic 3D display of a linear-polarizer type based on a FPR 3D panel with polarizing glasses. In this structure, the incident polarized light passes through the left side of the FPR cell without any change because the left patterned retarder has zero retardation. On the other hand, on the right side of the FPR, the light is changed to horizontally linear-polarized light by applying a $\lambda/2$ A-plate with an optical axis in the $+45°$ direction. Therefore, viewers wearing the polarized glasses can feel a binocular disparity between the two images with different polarization states from the FPR panel. However, the 3D image quality of the FPR 3D cell is deteriorated at an oblique viewing angle due to several problems of the optical retardation film. One is a shift in the optical axis in each optical film due to the changing polar angle θ and azimuth angle φ in the observation direction. The deviation angle δ, what is the effective angle from the optical axis of the A-film to the normal direction, can be expressed as [14]

$$\delta = \psi - \arcsin \times \left\{ \frac{\sin\phi_c \cos\phi_c \cos\theta_o - \cos\theta_c \sin\theta_o}{\left[1 - (\sin\phi_c \cos\phi_c \cos\theta_o + \cos\theta_c \cos\theta_o)^2\right]^{1/2}} \right\}, \quad (1)$$

where ϕ_c and θ_c are the azimuth and the polar angles, respectively, of the optical axis of the A-film and θ_o is the polar angle of the incident light for the anisotropic layer. The second reason is the change in the retardation value of the optical film in the oblique incidence. The change in retardation value in each optical film as a functions of the polar and the azimuth angles of the incident light can be easily calculated by using the extended 2×2 Jones matrix method [15–17]. The last factor is the dispersion of the refractive index of the optical films with wavelength [18]. The polarization states of the three primary colors (red, green, and blue) commonly differ from one another after the light passes through the retardation films due to dissimilar material and wavelength dispersion characteristics.

Figure 2(a) shows the changed polarization states of light for the right image in each viewing direction on the Poincaré sphere after passing through the FPR 3D cell. The symbols ◊, □, and ◯ in Fig. 2(a) express the polarization states of the light for blue ($B = 450$ nm), green ($G = 550$ nm), and red wavelengths ($R = 630$ nm), respectively. As shown in Fig. 2(a), the incident light from the start position, $-S_1$, rotates on the optical axis of position S_2 as much as the retardation value of the right patterned $\lambda/2$ A-film in the normal direction (black line). Thus, the green wavelength exactly reaches polarization position S_1, which is equal to a horizontally linear-polarization state; however, the blue and the red wavelengths obtain elliptical polarization states instead of linear polarization states due to phase dispersion. Light incident in the horizontal and the vertical directions (blue and red line, in Fig. 2(a)) will have a deviated optical axis δ compared to a normal viewing angle, so the optical direction of the right patterned film will deviate at positions A and B by (2δ from the position S_2, which is the optical axis of right patterned film in the normal direction. Therefore, the light passing through the FPR 3D cell for the right image reaches polarization positions $C_{i(i = r,\ g,\ \text{and}\ b)}$ and $D_{(i = r,\ g,\ \text{and}\ b)}$ along the blue and the red lines in the horizontal and the vertical directions, respectively.

Figure 2(b) show the calculated light leakage of the conventional FPR 3D structure for the right image for all visible wavelengths for various viewing angles. We confirmed serious light leakage for the conventional FPR 3D cell not only in the horizontal and the vertical directions but also in the blue and the red wavelength ranges caused by phase dispersion in normal direction. Consequently, the conventional FPR 3D cell can produce many ghost images due to deficient separation of the images in

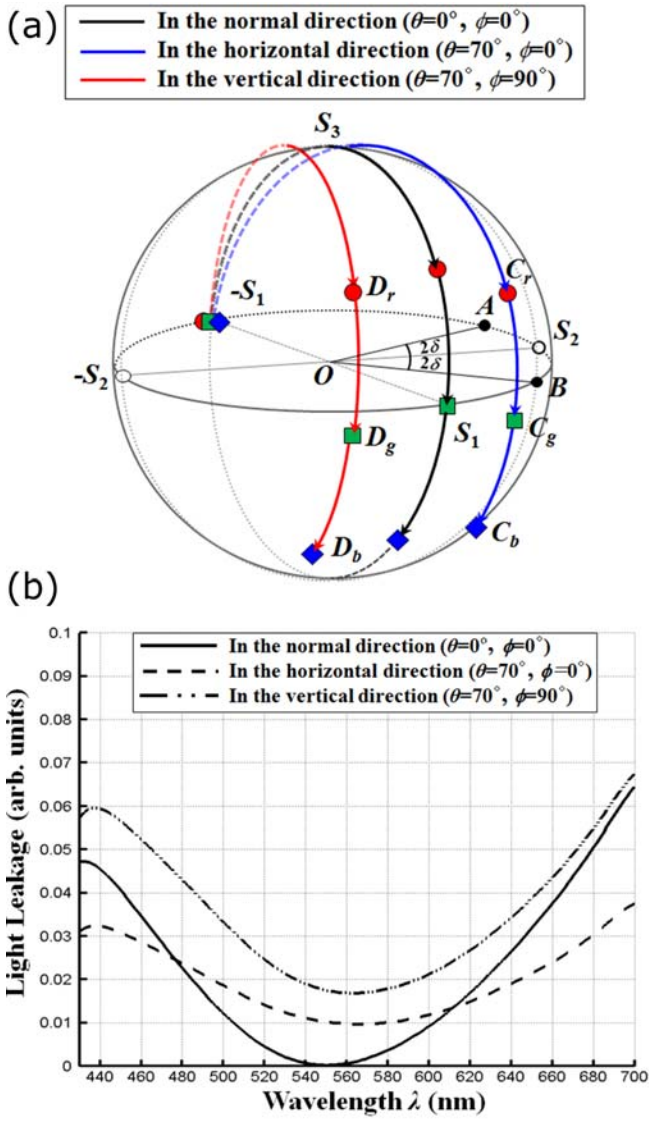

Fig. 2. (Color online) In the normal and the oblique directions ($\theta = 70°$, $\phi = 0°$ and $90°$), (a) the polarization path of the conventional structure on the Poincaré sphere for the right image and (b) the calculated light leakage of the conventional structure for the right image.

the normal and the oblique directions. Thus, if excellent 3D images are to be obtained in the oblique and the normal directions, these problems of degraded 3D image quality in the FPR 3D display must be overcome.

III. PROPOSED FPR 3D DISPLAY WITH A WIDEBAND AND WIDE VIEWING HALF-WAVE RETARDER

The left and the right images can be completely separated to vertically and horizontally linear polarization states over all visible wavelengths in both the normal

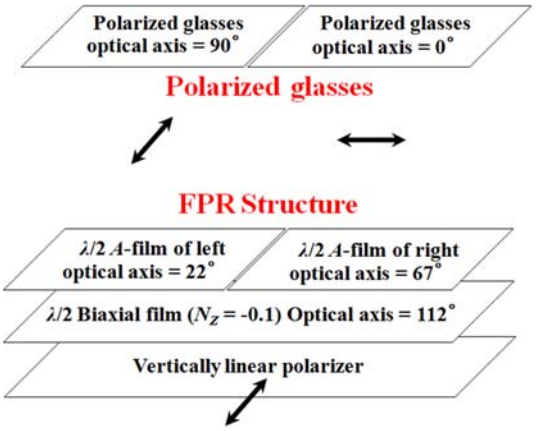

Fig. 3. (Color online) Proposed structure of the FPR 3D display with polarized glasses.

and the oblique directions by designing a FPR optical structure that has a wideband property in the normal direction and wide-viewing-angle property in the oblique direction (polar angle $\theta = 70°$, azimuth angle $\phi = 0°$ and $90°$, which is the target viewing angle for a medium-to large sized LCD panel). At first, the wideband property can be achieved by applying a wideband half-wave retarder that consists of a two positive $\lambda/2$ A-films. For the design of the wideband half-wave FPR cell, the optical axes of two $\lambda/2$ A-film must satisfy the wideband half-wave conditions $\phi_{\lambda/2\_1\text{st layer film}} = \phi_{\lambda/2\_2\text{nd layer film}} \pm 90°$ in the left image and $\phi_{\lambda/2\_1\text{st layer film}} = \phi_{\lambda/2\_2\text{nd layer film}} \pm 45°$ in the right image [19–21]. However, the use of only a wideband FPR 3D cell cannot produce outstanding 3D image quality because the optical parameters of each birefringence layer change, as described above, in the oblique direction. To resolve the problems, therefore, we added a wide-viewing-angle property to FPR 3D cell by using a $\lambda/2$ biaxial film instead of a conventional positive $\lambda/2$ A-film. In particular, a biaxial film can produce a excellent optical property in the oblique direction because it has the parameter $N_Z[= (n_x - n_z)/(n_x - n_y)]$, which can control the deviation angle δ by changing the N_Z factor [22,23].

Figure 3 shows the proposed optical structure for a FPR 3D cell with polarized glasses that can achieve wideband and wide-viewing-angle properties. This FPR 3D structure consists of a $\lambda/2$ biaxial film for the common part at the first layer and a positive $\lambda/2$ A-film for the patterned part at the second layer, as mentioned above. To design the FPR 3D structure, at first, we performed all the calculation, for the phase retardation of each film in the oblique direction by using the extended 2×2 Jones matrix method:

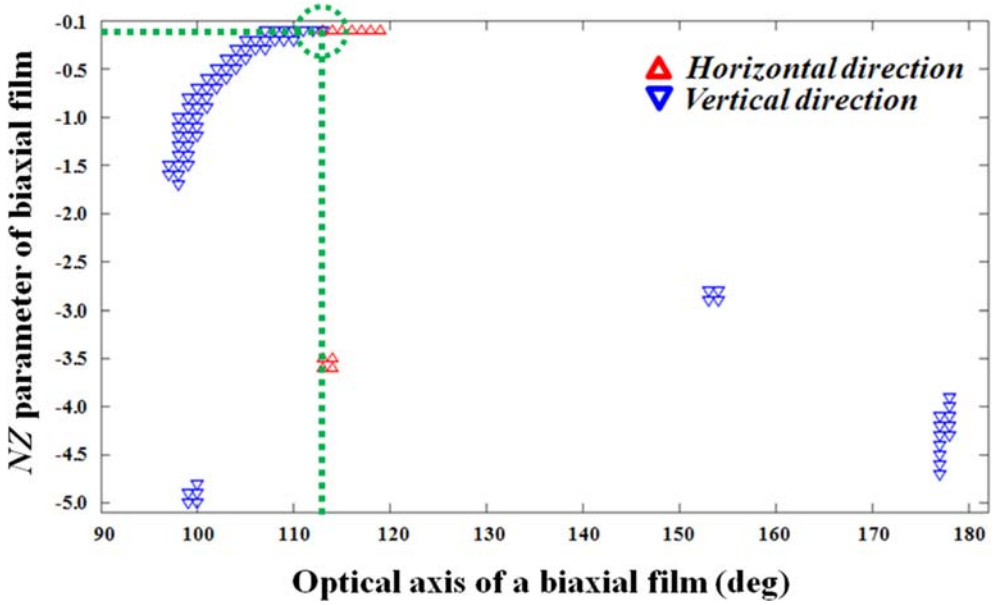

Fig. 4. (Color online) Parameter space map for the final polarization position of the FPR 3D cell as function of the optical axis and the N_Z factor of the biaxial film for the optimization.

$$\begin{aligned}\Gamma_{eff} &= (k_{z2} - k_{z1})d \\ &= k_0 \left[-\frac{\varepsilon_{xz}}{\varepsilon_{zz}} \frac{k_x}{k_0} + \frac{n_0 n_e}{\varepsilon_{zz}} \sqrt{\varepsilon_{zz} - \left(1 - \frac{n_e^2 - n_0^2}{n_e^2} \cos^2\theta \sin^2\phi\right) \left(\frac{k_x}{k_0}\right)^2} - \sqrt{n_0^2 - \left(\frac{k_x}{k_0}\right)^2} \right] d, \end{aligned} \tag{2}$$

where d represents the thickness of the film, and n_e and n_o represent the extraordinary and the ordinary refractive indices of the LC material, respectively. Also, we can calculate the changed polarization states after the incident light passes through each optical film in the normal and the oblique direction based on the Mueller matrix and the Stokes vector [24, 25]. The four Stokes parameters can usually be written as $S = (S_0, S_1, S_2, S_3)^T$, and the Mueller matrix of a rotated retarder can be described as follows [26]:

$$\begin{aligned} S_{final} &= R(-2\theta) \cdot M(\Gamma_{A+}) \cdot R(2\theta) \cdot S(Bi+) \\ &= \begin{pmatrix} 1 & 0 & 0 & 0 \\ 0 & \cos^2 2\theta + \cos\Gamma_{A+} \sin^2 2\theta & (1 - \cos\Gamma_{A+}) \sin 2\theta \cos 2\theta & \sin\Gamma_{A+} \sin 2\theta \\ 0 & (1 - \cos\Gamma_{A+}) \sin 2\theta \cos 2\theta & \sin^2 2\theta + \cos\Gamma_{A+} \cos^2 2\theta & -\sin\Gamma_{A+} \cos 2\theta \\ 0 & \sin\Gamma_{A+} \sin 2\theta & \sin\Gamma_{A+} \cos 2\theta & \cos\Gamma_{A+} \end{pmatrix} \begin{pmatrix} S_{0Bi} \\ S_{1Bi} \\ S_{2Bi} \\ S_{3Bi} \end{pmatrix} = \begin{pmatrix} S_{0\_final} \\ S_{1\_final} \\ S_{2\_final} \\ S_{3\_final} \end{pmatrix}, \end{aligned} \tag{3}$$

where S_{final} represents the Stokes vector of the output light, $S(Bi+)$ is the Stokes vector of the incident light after passing through the $\lambda/2$ biaxial film, Γ_{A+} is a retardation of the patterned positive A-film, $R(2\theta)$ and $R(-2\theta)$ are the rotating matrix and reverse-rotating matrix to the principal axis, respectively, and $M(\Gamma_{A+})$ depicts the Muller matrix for rotated polarizing components with phase retardation Γ_{A+}. When the light passes through the right and the left patterned $\lambda/2$ A-film layers in the oblique direction, the ideal final polarization states of the light have to become horizontally and vertically linear polarization, which is equal to S_{final} (1, ±1, 0, 0) at the Stokes vector. As mentioned above, however, the final polarization position of the light passing through the FPR 3D structure is rotated to an elliptical polarization position due to several optical problems of the anisotropic medium layer such as a change of the optical axis and a retardation in the oblique direction. Thus,

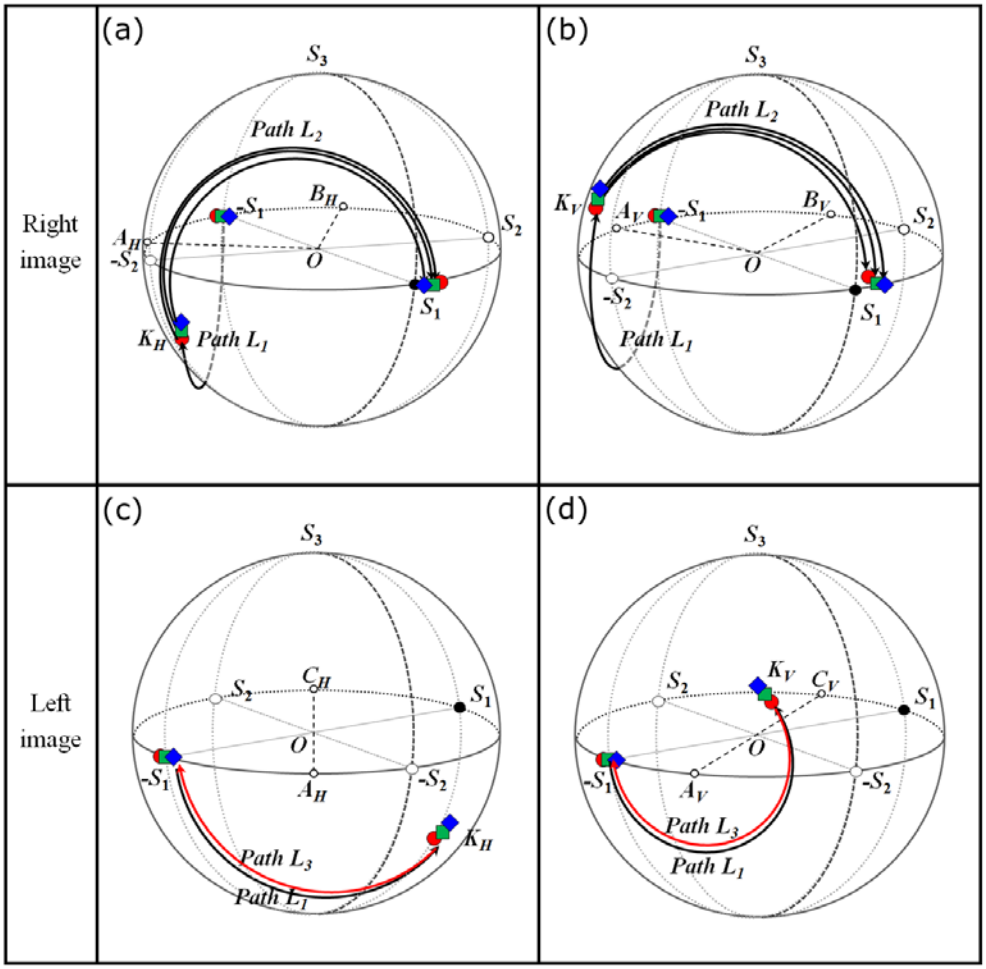

Fig. 5. (Color online) Polarization states of the proposed configuration on the Poincaré sphere: the polarization path for right image (a) in horizontal direction and (b) in vertical direction, and that for the left image (c) in horizontal direction and (d) in vertical direction.

we used the parameter square method to find the optimized value of the parameter that not only could satisfy the wideband half-wave relationship and but also could produce completely linear polarization states of the left and the right images at horizontal and vertical viewing angles simultaneously. Figure 4 shows a two-dimensional parameter space map for the optimization of the FPR 3D structure. If the optimization condition for the optical parameters of a $\lambda/2$ biaxial film is to be found, the final polarized light should simultaneously have values of the positions $\pm S_1$ between ± 0.994 and ± 1 in the horizontal and the vertical directions. For, the optimized condition, the optical axis was 112°, and the N_Z factor had a value of -0.1 for the $\lambda/2$ biaxial film, as shown Fig. 4. In addition, the optical axes of the right and the left patterned $\lambda/2$ A-films were 67° and 22°, respectively, based on the wideband half-wave relationship.

Figure 5 shows how this proposed structure produces the linear polarization states on the Poincaré sphere after the light passes through the two designed $\lambda/2$ films in the horizontal and the vertical direction. In Fig. 5(a), the starting position is position $-S_1$ when the light passes through the vertical polarizer in the horizontal direction. Then, the polarization state of the light passing through the $\lambda/2$ biaxial film, which has the optical axis at the position A_H $(112° + 2\delta_{(\phi=0°)})$, moves to position K_H along the path L_1. The polarization of light passing through the right patterned $\lambda/2$ A-film, which has the optical axis at the position B_H $(67° + 2\delta_{(\phi=0°)})$, moves to final polarization position S_1 along the path $L2$. The effective retardation of films is changed to 2.6444 rad for the biaxial $\lambda/2$ film and 3.7859 rad for the right patterned $\lambda/2$ A-film in the horizontal direction while the retardation values of two films are 3.1416 rad in the normal direction. However the two films compensate for each other because of their optimized designs. Then, the proposed structure leads to a perfect horizontally linear polarization for the right image in the horizontal direction.

Figure 5(b) expresses the polarization path of the proposed configuration for the right image in the vertical direction. Although the optical axes of the biaxial $\lambda/2$ film and the right patterned $\lambda/2$ A-film change to the po-

Table 1. Calculated optimized dispersion properties of the optical anisotropy of optical uniaxial films.

	$\Delta n/\Delta n$ (550 nm)		Δnd [nm]
	450 nm	630 nm	550 nm
Left FPR $\lambda/2$ A-film	0.829	1.13	275
Right FPR $\lambda/2$ A-film	0.816	1.15	275

Table 2. Calculated optimized dispersion properties of optical anisotropy of the optical biaxial films.

	$\Delta n/\Delta n$ (550 nm) $(\Delta n = n_x - n_y, n_z - n_y)$		Δnd [nm] $(\Delta n = n_x - n_y)$
	450 nm	630 nm	550 nm
biaxial $\lambda/2$ film	1.0005	1	276

sitions A_V ($112^\circ + 2\delta_{(\phi=90^\circ)}$) and B_V ($67^\circ + 2\delta_{(\phi=90^\circ)}$) and the retardation is 3.8168 rad and 2.6898 rad, the polarization path is in accord with the horizontal viewing angle on Poincaré sphere. As a result, we obtained the optimized values for the final polarization position S_1: 0.9971 (B), 0.996 (G), and 0.9945 (R) in the horizontal direction and 0.9954 (B), 0.9966 (G), and 0.9974 (R) in the vertical direction. On the other hand, Figs. 5(c) and (d) show the polarization paths of the proposed configuration for the left image in the horizontal and the vertical directions, respectively. In the case of the left image, the polarization state should stay at the start position $-S_1$ after the light passes through the final retardation film layer in order to separate to vertically linear polarization. Therefore, the optical axis of the left patterned $\lambda/2$ A-film should be about 90° from the optical axis of the $\lambda/2$ biaxial film in order to return to the starting position $-S_1$. As shown Figs. 5(c) and (d), we can confirm arrival at the final position $-S_1$ after the light passes through the left patterned $\lambda/2$ A-film has rotated on the optical axis of position C_H ($22^\circ + 2\delta_{(\phi=0^\circ)}$) and C_V ($22^\circ + 2\delta_{(\phi=90^\circ)}$) along the path L_3 from position K_H and K_V in the horizontal and the vertical directions. As a result, we obtained the optimized values of the final polarization position $-S_1$: -0.9994 (B), -0.9996 (G), and -0.9997 (R) in the horizontal direction and -1 (B), -1 (G), and -0.9999 (R) in the vertical direction. Tables 1 and 2 show the calculated optimized retardation values for R, G, and B wavelengths of each optical film used.

IV. CALCULATED RESULTS AND DISCUSSION

FPR stereoscopic 3D displays simultaneously provide left and right images to the eyes of a viewer wearing eyeglasses with orthogonal linear polarizations, and 3D images are constructed. However, this FPR 3D cell can produces crosstalk that induces ghost images caused by

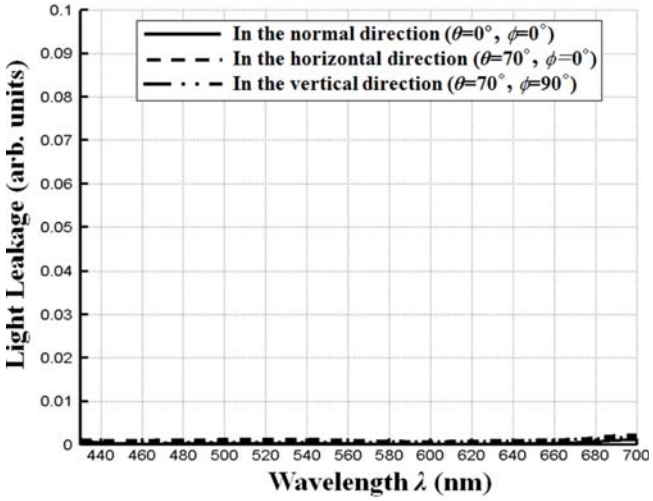

Fig. 6. Calculated light leakages of the proposed structure in the normal and the oblique directions ($\theta = 70^\circ$, $\phi = 0^\circ$ and 90°) for the entire visible wavelength spectrum.

light leakage when the final polarized light of the left and the right image is transmitted to opposite polarized glasses in the oblique direction. Therefore, we calculate the light leakage and the crosstalk in order to verify the optical performance of the proposed FPR 3D structure.

Figure 6 shows the calculated light leakage of the proposed FPR 3D structure for the entire visible wavelength range at normal, horizontal, and vertical viewing angles. The conventional FPR 3D structure experience serious light leakage as shown Fig. 2(b). However, the proposed structure maintains an excellent dark state for the entire visible wavelength spectrum not only in the normal direction but also in the horizontal and the vertical directions.

Figures 7 and 8 show the calculated crosstalks of the proposed configuration, compared to those of the conventional structure, in the horizontal and the vertical directions, respectively. The crosstalk value can be defined as [27]

$$3D\,Crosstalk_{Left(Right)} = \frac{R(L)\_dark}{L(R)\_bright} \times 100\ [\%]. \quad (4)$$

Here, $L(R)\_bright$ is the luminance of the left and the right eyes at the bright states, and $R(L)\_dark$ is the luminance of the left and the right eyes at the dark states. We confirmed that the proposed optical structure improved the left 3D crosstalk by about 91.87% in the horizontal direction and by about 97.22% in the vertical direction as shown in Fig. 7(a) and Fig. 8(a), respectively. On the other hand, the right 3D crosstalk optimized for not only the proposed FPR 3D cell but also the conventional FPR 3D cell because the conventional structure could produce ideal vertically-linear polarization; the designed lack of retardation produced no change in the polarization property of the left FPR. Thus, as shown in Figs. 7(b) and 8(b), the proposed FPR 3D structure has the same 3D

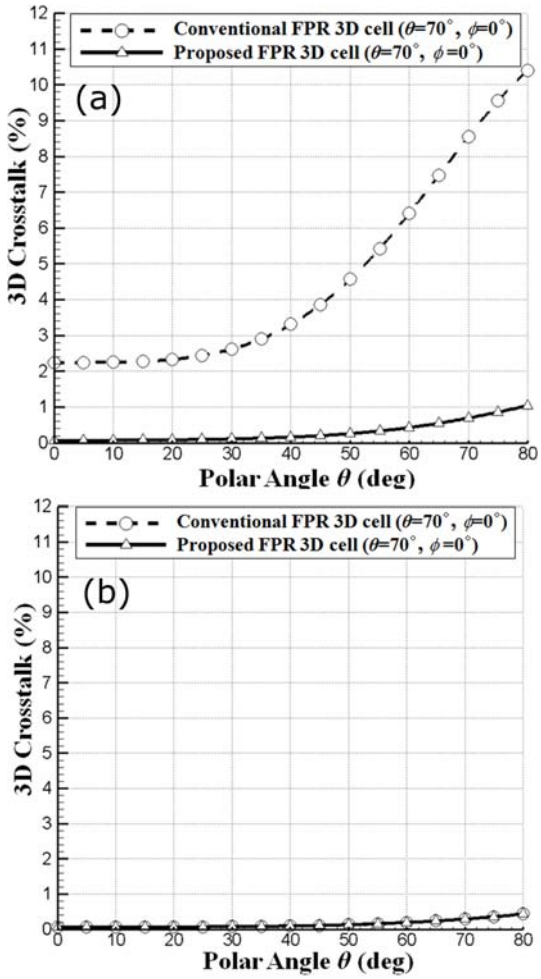

Fig. 7. Comparison of the calculated 3D crosstalk of the conventional and the proposed FPR 3D structures in the horizontal direction: (a) for the left 3D crosstalk and (b) for the right 3D crosstalk.

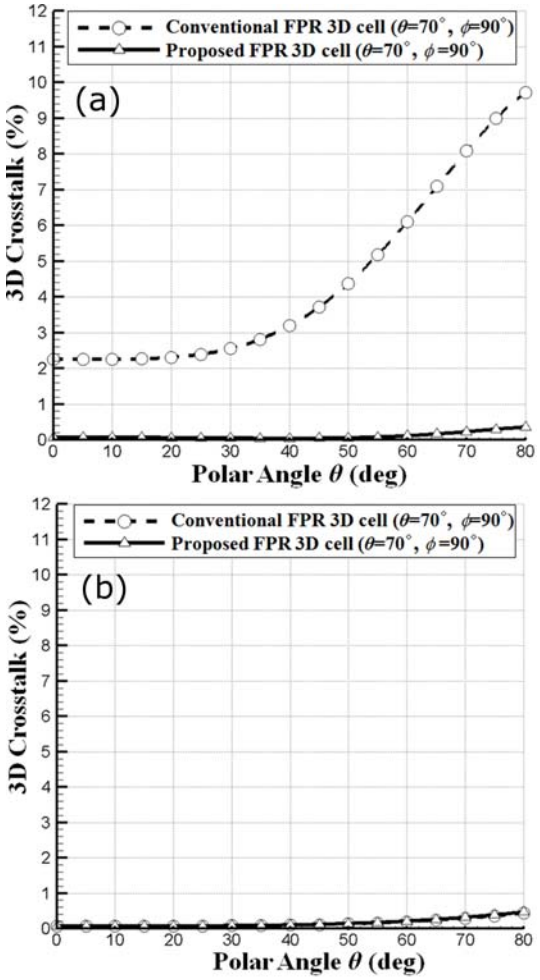

Fig. 8. Comparison of the calculated 3D crosstalk of the conventional and the proposed FPR 3D structures in the vertical direction: (a) for the left 3D crosstalk and (b) for the right 3D crosstalk.

crosstalk in the horizontal and the vertical directions as the conventional structure.

V. CONCLUSION

In summary, we have designed an optical structure for a FPR 3D display that can be used to satisfy the optical properties of wideband image quality and wide-viewing angle in the oblique direction. We calculated the retardation of each film and analyzed the polarization states of the light passing through the FPR 3D cell in the oblique direction by using the Mueller matrix method. Then, we optimized an optical parameter for a biaxial $\lambda/2$ film and patterned $\lambda/2$ A-film based on the parameter space method as a function of the optical axis and the N_Z factor of a biaxial film and on the wideband half-wave relationship. We demonstrated good optical performances of the proposed FPR 3D structure by effectively improving the 3D crosstalk in the oblique direction. We are confident that the proposed FPR 3D display will be an outstanding technology that will allow high-quality 3D images and wide viewing angles to be achieved.

ACKNOWLEDGMENTS

This research was supported by Dong-A University.

REFERENCES

[1] S. Pastoor and M. Wopking, Displays **17**, 100 (1997).
[2] D. Matsunaga, T. Tamaki, H. Akiyama and K. Ichimura, Adv. Mater. **14**, 1477 (2002).
[3] J.-C. Liou, K. Lee and F.-G. Tseng, in *Digest of Technical Papers of the 8th International Meeting on Information Display* (IMID, Ilsan, Korea, 2008), p. 710.

[4] D. Suzuki *et al.*, SID Int. Symp. Dig. Tec. Pap. **40**, 428 (2009).
[5] C.-H. Tsai, W.-L. Chen and W.-L. Hsu, SID Int. Symp. Dig. Tec. Pap. **39**, 456 (2008).
[6] Y.-J. Wu, Y.-S. Jeng, P.-C. Yeh, C.-J. Hu and W.-M. Huang, SID Int. Symp. Dig. Tec. Pap. **39**, 260 (2008).
[7] J. H. Oh, W. H. Park, B. S. Oh, D. H. Kang, H. J. Kim, S. M. Hong, J. H. Hur and J. Jang, SID Int. Symp. Dig. Tec. Pap. **39**, 444 (2008).
[8] H. Hong, D. Lee, J. Jang and M. Lim, in *Digest of Technical Papers of the 9^{th} International Meeting on Information Display* (IMID, Ilsan, Korea, 2009), p. 1010.
[9] J.-H. Lee, H. Choi, S. H. Lee, J. C. Kim and G.-D. Lee, Appl. Opt. **45**, 7279 (2006).
[10] J.-H. Lee, J.-H. Son, S.-W. Choi, W.-R. Lee, K.-M. Kim, J. S. Yang, J. C. Kim, H. Choi and G.-D. Lee, J. Phys. D: Appl. Phys. **39**, 5143 (2006).
[11] S.-H. Ji and G.-D. Lee, Liq. Cryst. **36**, 657 (2009).
[12] Y. J. Lim, B. C. Kim, Y. J. Choi, S. H. Lee, W.-S. Kang and G.-D. Lee, Liq. Cryst. **39**, 675 (2012).
[13] W. S. Kang, B.-J. Mun, G.-D. Lee, J. H. Lee, B. K. Kim, H. C. Choi, Y. J. Lim and S. H. Lee, J. Appl. Phys. **111**, 103119 (2012).
[14] T. W. Ko, J. C. Kim, H. C. Choi, K. H. Park, S. H. Lee, K.-M. Kim, W.-R. Lee and G.-D. Lee, Appl. Phys. Lett. **91**, 053506 (2007).
[15] A. Lien, Appl. Phys. Lett. **57**, 2767 (1990).
[16] X. Zhu, Z. Ge and S.-T. Wu, J. Disp. Technol. **2**, 2 (2006).
[17] D.-K. Yang and S.-T. Wu, *Fundamentals of Liquid Crystal Devices* (John Wiley & Sons Ltd., Chichester, 2006).
[18] Y. Fujimura, T. Kamijo and H. Yoshimi, in *Proceeding of the SPIE* (Santa Clara, Calif, USA, 2003), p. 96.
[19] T.-H. Yoon, G.-D. Lee and J. C. Kim, Opt. Lett. **25**, 1547 (2000).
[20] G.-D. Lee, G.-H. Kim, T.-H. Yoon and J. C. Kim, Jpn. J. Appl. Phys. **39**, 2716 (2000).
[21] G.-D. Lee *et al.*, Jpn. J. Appl. Phys. **39**, L221 (2000).
[22] J.-S. King, W.-T. Whang, W.-C. Lee and L.-M. Chang, Jpn. J. Appl. Phys. **45**, L501 (2006).
[23] C.-H. Lin, Opt. Express **16**, 13276 (2008).
[24] J. E. Bigelow and R. A. Kashnow, Appl. Opt. **16**, 2090 (1977).
[25] K. Vermeirsch, A. D. Meyere, J. Fornier and H. D. Vleeschouwer, Appl. Opt. **38**, 2775 (1999).
[26] D. Goldstein, *Polarized Light* (Marcel Dekker, New York, 2003), Chap. 5.4, p. 75.
[27] P.-C. Yeh, C.-W. Chen, C.-I. Huang, Y.-J. Wu, C.-H. Shih and W.-M. Huang, SID Int. Symp. Dig. Tec. Pap. **40**, 1431 (2009).